Nonlinear Properties of Tapered Laser Cavities

Slawomir Sujecki, Luis Borruel, James Wykes, Pablo Moreno, Bernd Sumpf, Phillip Sewell, Hans Wenzel, Trevor M. Benson, Goetz Erbert, Ignacio Esquivias, and Eric C. Larkins

***Abstract*—The nonlinear phenomena accompanying the process of light generation in high-power tapered semiconductor lasers are studied using a combination of simulation and experiment. Optical pumping, electrical overpumping, filamentation, and spatial hole burning are shown to be the key nonlinear phenomena influencing the operation of tapered lasers at high output powers. In the particular tapered laser studied, the optical pumping effect is found to have the largest impact on the output beam quality. The simulation model used in this study employs the wide-angle finite-difference beam propagation method for the analysis of the optical propagation within the cavity. Quasi-three-dimensional (3-D) thermal and electrical models are used for the calculation of the 3-D distributions of the temperature, electrons, holes, and electrical potential. The simulation results reproduce key features and the experimental trends.**

***Index Terms*—Beam propagation modeling, high-brightness lasers, laser resonators, optical beams, semiconductor lasers.**

I. Introduction

MANY applications in the fields of telecommunications [1], medicine [2], printing, and manufacturing [3] require the use of a high-brightness coherent optical beam from a low-cost reliable source. High-power semiconductor lasers offer the advantages of small size, high efficiency, reduced cost, and improved reliability compared with solid-state and gas lasers. Conventional broad-area high-power laser diodes suffer from poor beam quality, but recently, work on high-brightness laser diodes has shown that the beam quality can be improved significantly with an appropriate device design. A number of high-brightness laser diode concepts have been proposed, including broad-area lasers with a profiled facet reflectivity [4], phase-locked structures [5], antiguided waveguide arrays [6], α-grating distributed feedback lasers [7], master oscillator power amplifier (MOPA) lasers [8], unstable resonator lasers [9], external cavity lasers [10], and tapered lasers [11], [12] (Fig. 1). Tapered lasers have received the greatest attention because of their simplicity and compatibility with the fabrication processes used to make commercial high-power laser bars. The numerical analysis of the properties of tapered laser diode properties is the subject of this paper.

Manuscript received December 15, 2002; revised June 3, 2003. This work was supported by the European Commission under the IST project 1999-10356, ULTRABRIGHT.

S. Sujecki, J. Wykes, P. Sewell, T. M. Benson, and E. C. Larkins are with the School of Electrical and Electronic Engineering, University of Nottingham, Nottingham NG7 2RD, U.K. (e-mail: eezss@gwmail.nottingham.ac.uk).

L. Borruel, P. Moreno, and I. Esquivias are with the Departamento de Tecnología Fotónica, Universidad Politécnica de Madrid, Madrid 28040, Spain.

B. Sumpf, H. Wenzel, and G. Erbert are with the Ferdinand Braun Institut für Höchstfrequenztechnik, D-12489 Berlin, Germany.

Digital Object Identifier 10.1109/JSTQE.2003.818843

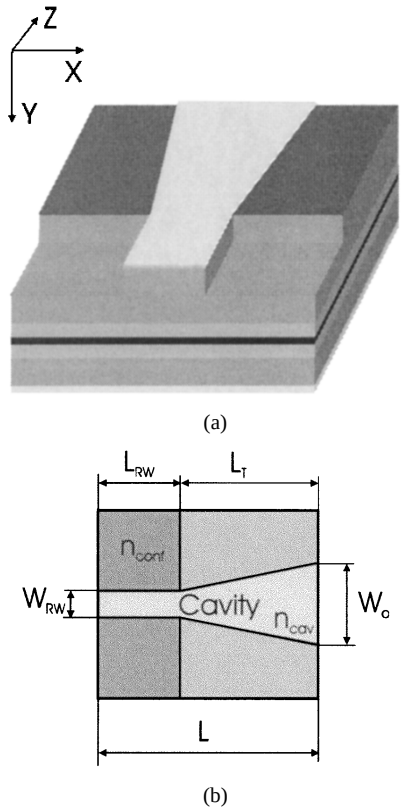

Fig. 1. (a) Generalized tapered laser structure and (b) its two-dimensional effective index representation.

A tapered laser consists of a straight waveguide section and a tapered amplifier section, as shown in the schematic diagram in Fig. 1. The straight waveguide section (sometimes accompanied by a beam spoiler) plays a key role and serves as a modal filter, ensuring that the tapered amplifier is only excited by the fundamental transverse mode of the straight waveguide. The tapered amplifier section allows the optical beam to expand gradually in order to lower the optical power density. This minimizes the intensity of detrimental effects [e.g., spatial hole burning (SHB)], allows an increase in the total output power, and increases the catastrophic optical mirror damage (COMD) threshold. The straight waveguide section also defines the (unperturbed) shape of the desired virtual source point in the cavity and the rate of lateral beam divergence in the tapered amplifier. Undesirable power-dependent changes in the shape and position of the virtual point source are caused by the carrier- and temperature-induced refractive index perturbations occurring in the resonant cavity, resulting in a decrease in beam quality (i.e., M^2, beam parameter product), brightness, and "wandering astigmatism."

A number of papers have been published on various aspects of high-power tapered laser and amplifier design, including the dependence of the beam quality on the tapered cavity geometry at low powers [13], the influence of the carrier and temperature distribution [14], [15], filamentation processes [16], the spatio-temporal dynamics of carriers and photons [17], and electron leakage [18]. Several research groups have demonstrated tapered lasers with multiwatt high-quality beams [19], [20], but there is still a need to understand and predict the behavior of these devices more accurately.

In order to further optimize tapered semiconductor lasers, laser manufacturers need both efficient design tools and a detailed understanding of the complex interactions between the optical, electronic, and thermal processes occurring during self-focusing, filamentation, and SHB. Such design tools must be compatible with the current generation of PCs and standard workstations in terms of speed and memory, so that fast and reliable simulations can be performed. Thus, although considerable progress has been made in time-domain analysis of laser diodes [17], [21]–[25], such models require computational resources, which are well beyond the capabilities of common computers. This is particularly true for the simulation of high-power lasers with long (2–4 mm) and wide (20–300 μm) resonators. Furthermore, although the results of time-domain models are more comprehensive, they are also much more difficult to interpret. On the other hand, steady-state models are computationally more tractable and allow tracking of the beam propagation, making the steady-state nonlinear photon-carrier-temperature interactions in the resonator easier to understand. This paper describes the development of such a design tool and its application to the study of filamentation, SHB, current spreading, optical pumping, and electrical overpumping effects in high-power tapered lasers. To model the beam propagation in the presence of local temperature- and carrier-induced index perturbations with reasonable computational resources, a static single-wavelength model based on the wide-angle finite-difference beam propagation method (WA FDBPM) has been developed. This model solves the optical, electrical, and thermal equations for tapered lasers, taking into account the carrier- and temperature-induced refractive index changes. By relaxing the phase-matching condition at the back facet, the present model effectively maps the time-average of all of the optical fields onto a steady-state field distribution with a single wavelength. Thus, the results of this model can best be compared with the time average of the results of more comprehensive time-domain models over a suitably long time span. The price paid for this gain in computational efficiency is the loss of the ability to reproduce time-dependent four-wave mixing and spectral hole-burning effects. Thus, although the model cannot be used to analyze dynamic modal instabilities or to reproduce subtle dynamic asymmetries in the near-field pattern [22], it is able to predict those properties of high-brightness laser diodes that are most important to high-power laser manufacturers (e.g., beam-divergence, virtual point source profile, astigmatism, etc.) and identify the origins of filamentation and SHB.

SHB and filamentation effects have received a fairly comprehensive treatment for semiconductor lasers in general [27] and tapered laser and amplifier structures in particular (both experimentally [28], [29] and theoretically [14]–[17], [30], [31]). Consequently, in this paper, SHB and filamentation effects in the simulation results are noted clearly but not discussed further. Instead, this paper focuses on showing how filamentation and SHB are triggered by optical pumping and electrical overpumping. Optical pumping and electrical overpumping are well known to the semiconductor laser community, although the lack of common nomenclature brings about some confusion. For example, electrical overpumping is also known as lack of Fermi level pinning [32] and can be influenced by current profiling techniques such as tailored injection and the use of distributed electrodes [33]. Similarly, optical pumping is often referred to as photon transport or optical bleaching [26] and plays a key role in saturable absorbers [34]. To the best of our knowledge, however, little attention has been given to the investigation of the roles of optical pumping and electrical overpumping on SHB and filamentation in tapered lasers. Therefore, it is one of the goals of this paper to produce a detailed understanding of these interactions.

Section II provides the details of the model used. This is followed in Section III by a discussion of the simulation results for 732-nm GaAs-based tapered lasers and their comparison with the experimental observations. Light with a wavelength of 732 nm is suitable for photodynamic cancer therapy, which is an important target application for these high-brightness laser diodes.

II. Simulation Model

The properties of a semiconductor laser are described by the distributions of the electromagnetic fields, the hole and electron concentrations, the electrical potential, and the temperature. Under steady-state operating conditions, the optical field distribution is obtained from the solution of the vectorial wave equations

$$\nabla^2 H + \frac{\nabla \varepsilon}{\varepsilon} \times (\nabla \times H) = \mu_0 \varepsilon \omega H \tag{1a}$$

$$\nabla^2 \mathrm{E} + \nabla \left(\mathrm{E} \times \frac{\nabla \varepsilon}{\varepsilon} \right) = \mu_0 \varepsilon \omega \mathrm{E} \tag{1b}$$

where μ_0 is the magnetic permeability of the free space, ω is the angular frequency, and ε is the dielectric constant. The dielectric constant depends on the temperature and carrier distributions. The carrier concentrations in the laser cavity are determined by self-consistently solving the current continuity equations for electrons and holes with the Poisson equation

$$\nabla \mathbf{j}_n - q\left(R_{\mathrm{nr}} + R_{\mathrm{sp}} + F_n^{\mathrm{qw}}\right) = 0 \tag{2a}$$

$$\nabla \mathbf{j}_p + q\left(R_{\mathrm{nr}} + R_{\mathrm{sp}} + F_p^{\mathrm{qw}}\right) = 0 \tag{2b}$$

$$\nabla(\varepsilon_s \nabla \phi) + q(p - n + N_D - N_A) = 0 \tag{2c}$$

where R_{nr} and R_{sp} are, respectively, the nonradiative and spontaneous recombination rates in bulk regions, and other symbols have their usual meanings. The terms F_n^{qw} and F_p^{qw} appearing in the continuity equations account for the carrier capture/escape rates between the confined and unconfined states in the

quantum wells (QWs), and can be expressed as (see [39]–[41] for details)

$$F_n^{\mathrm{qw}} = \frac{n_{3\text{–D}}}{\tau_{\mathrm{cap}}^n}\left[1 - \exp\left(\frac{E_{\mathrm{fn}}^{2\text{–D}} - E_{\mathrm{fn}}^{3\text{–D}}}{kT}\right)\right]$$

where ${\tau_{\mathrm{cap}}}^n$ is the electron capture time. A similar expression describes the hole capture/escape rate.

Two additional continuity equations are solved in each QW

$$\int_{\mathrm{qw}} F_n^{\mathrm{qw}} dv - R_{\mathrm{nr}}^{\mathrm{qw}} + R_{\mathrm{sp}}^{\mathrm{qw}} + R_{\mathrm{st}} = 0$$

$$\int_{qw} F_p^{\mathrm{qw}} dv - R_{\mathrm{nr}}^{\mathrm{qw}} + R_{\mathrm{sp}}^{\mathrm{qw}} + R_{\mathrm{st}} = 0$$

where $R_{\mathrm{nr}}^{\mathrm{qw}}$, $R_{\mathrm{sp}}^{\mathrm{qw}}$, and R_{st} denote the nonradiative, spontaneous, and stimulated recombination rates in QW regions.

The temperature distribution in the cavity is calculated by solving the heat conduction equation

$$\nabla(-\kappa \nabla T) = W \tag{3}$$

where κ is the thermal conductivity and W is the heat generation rate.

The electrical and thermal models used are described in more detail in [35]–[38], and only a brief description is given here. The current densities in (2) include standard drift-diffusion terms together with the term arising from thermal gradients. Fermi–Dirac statistics is considered for two-dimensional (2-D) carriers in QW, and Boltzmann statistics for carriers in bulk regions. A parabolic band approximation is used for the gain after fitting the band parameters to complete band-mixing calculations for the valence band at the beginning of the simulation. The local material gain is calculated with a Lorentzian linewidth broadening function at the lasing wavelength as a function of the local temperature and electron and hole concentrations. Spontaneous emission, Shockley–Read–Hall, and Auger recombination rates are calculated using standard expressions [42], taking into account temperature dependencies. Free carrier absorption and bandgap renormalization are included by means of empirical formulations [42]. The thermal model considers Joule, nonradiative recombination, and absorption by free-carriers as local heat sources in (3), together with the so-called "excess power" needed to fulfill energy conservation [36].

Wenzel *et al.* used 8×8 $k \cdot p$ calculations to show that near the gain maximum, the real part of the refractive index perturbation of the quantum well is proportional to the square root of the carrier density [43]. This was confirmed experimentally and, therefore, this dependence was included in the model. The temperature dependence of the real part of the refractive index is also included [36].

In general, ε [in (1)] is a function of the temperature and carrier distributions, which in turn depend on the optical field intensity and the injection current. Thereafter, (1)–(3) form a coupled nonlinear system. Due to the complex form of this system, the solution of these coupled nonlinear equations is difficult and results in prohibitive calculation time and memory requirements for the current generation of computers. Fortunately, polarization coupling can be neglected in the first-order approximation while studying SHB and filamentation. This allows the use of the semivectorial version of (1)

$$\nabla^2 \Psi - \mu_0 \varepsilon k_0^2 \Psi = 0 \tag{4}$$

in each region of constant dielectric constant, together with appropriate boundary conditions [44]. In (4), k_0 is the wave number, Ψ is one of the transverse electric field components, and $|\Psi|^2$ is proportional to the photon density. Equation (4) is the standard nonlinear wave equation commonly used for nonlinear optics and can be solved with procedure analogous to the use of subsequent Born approximations [34], i.e., solving first (4) with $\varepsilon = \varepsilon(|\Psi|^2 = 0)$. Equations (2) and (3) are solved next, and the dielectric constant distribution is modified according to the new temperature and carrier distributions. The longitudinal carrier and heat fluxes have been neglected in these quasi-three-dimensional (3-D) calculations. This approximation is reasonable due to the slowly varying longitudinal structure. Furthermore, we have checked the validity of this assumption for the structures under consideration by comparing the simulation results with full 3-D electrical and thermal simulations. In the case of the longitudinal carrier flow, no difference was observed, consistent with the electrical slice separation (100 μm), which is much higher than the carrier diffusion length. For the longitudinal flow of heat, although the longitudinal gradient is smoother in a fully 3-D model, the lateral profiles (responsible for the refractive index induced change) are not significantly modified. Next, (4) is solved again and the process is continued until the photon distribution in the cavity converges to a stable solution. In each iteration, the wave (4) is solved using the WA FDBPM algorithm [13], [45], [46]. The effective index approximation has been used to reduce the original 3-D structure to a 2-D one (Fig. 1) to improve the computational efficiency.

The solution of (2)–(4) has been performed using the coupled solution method (CSM) rather than with the conceptually simpler separate solution method (SSM) [45]. Thus, the CSM provides improved stability and faster convergence when compared with SSM [45]. The CSM algorithm is described in Fig. 2. In the SSM, the analysis is initiated at the rear facet and the optical field is propagated along an entire round trip of the cavity, yielding a new photon density distribution. Subsequently, (2) and (3) are solved for each 2-D slice (perpendicular to the longitudinal axis) using the new photon distribution to obtain new carrier, potential, and temperature distributions in the cavity. These new carrier and temperature profiles are used to update the lateral gain and refractive index distributions, which are then used in (4) to obtain a new photon distribution. This process is repeated until the shape and power of the reflected field at the back facet converges. The CSM operates in a similar manner, except that the electronic and thermal equations are solved at each slice and the resulting updated refractive index and gain and profiles in the slice are used for the optical propagation to the next slice (Fig. 2). As the information about photon, carrier, and temperature is updated at every step rather than after a full round trip of the cavity, the CSM helps to avoid the large cumu-

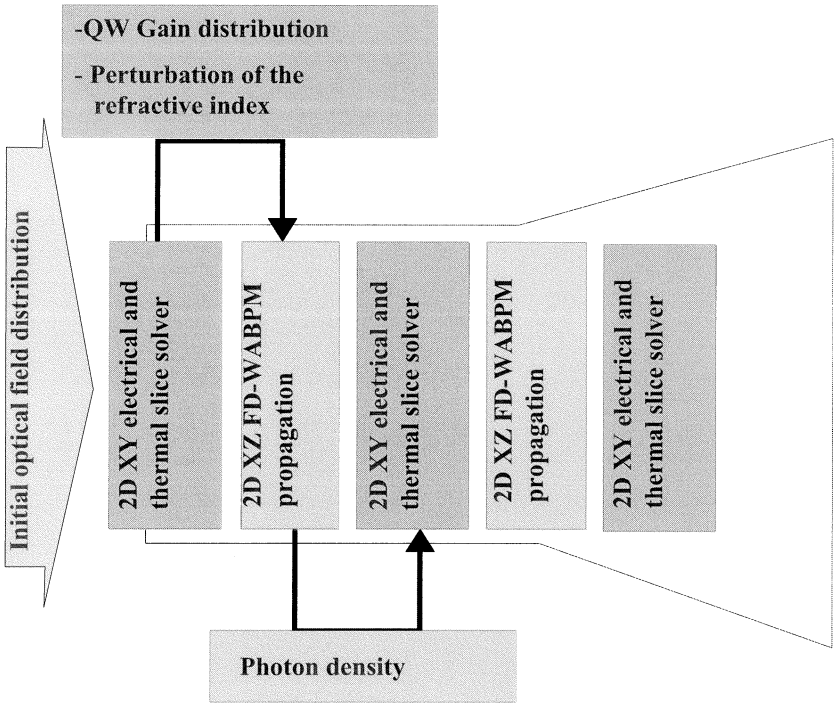

Fig. 2. Flowchart used by the WA FDBPM cavity analysis technique.

lative errors that appear in the SSM. This problem is particularly acute in high-power taper lasers due to the large cavity length.

The phase of the incoming wave has not been considered in the convergence criterion described above. As a consequence, there is a significant gain in the computational efficiency but the opportunity to analyze the lasing spectrum and spectral hole burning is lost. Thus, the problem arises of how to select the wavelength at which the calculations are carried out. In this work, the emission wavelength was taken to be that of the gain maximum at each current, calculated from one-dimensional (1-D) simulations for a broad-area laser with same area as the tapered laser under study.

Facet reflectivity calculations were performed using a free space radiation method (for unguided waves in the coating) coupled with the finite-difference beam propagation method (for the guided waves in the semiconductor) [48]. These calculations indicate that the use of simple reflection coefficients is satisfactory for the structures studied here and only need to be calculated accurately once at the beginning of the simulation. We have also found that the use of the Padé (1,1) wide angle scheme [47] suffices to properly treat the beam propagation in the tapers studied. The analysis of beam spoilers has also been included by using the simplified approach employed by Mariojouls [15], in which the fields impinging on the beam spoilers are completely absorbed.

The software directly produces the optical field, carrier, electrical potential, and temperature distributions in the cavity. In order to extract more information from the results, extensive post-processing analysis of these data is essential. The following figures of merit are evaluated from the simulations results, using the extensive post-processing analysis tools developed for this laser design tool: lateral far-field profile; lateral beam divergence; lateral size, position, and distribution of the virtual point source; and M^2. The far-field profile is calculated by taking the Fourier transform of the near-field distributions at the front facet and performing a steepest descent path calculation [49]. The beam divergence is determined from the far-field profile, using both of the standard definitions (full-width at half-maximum and e^{-2}). The virtual point source is obtained by performing a Fourier transform on the front facet near-field distribution and analytically back-propagating the resulting spectrum, as if it existed in free space, until the beam waist is found. The width of the waist is calculated using the $1/e^2$ definition. The power in the central lobe of the virtual source (i.e., at the beam waist) is the power integrated between the points at which the power density drops to 10% of its maximum value. For the determination of M^2, the ratio of the beam divergence to that of an ideal Gaussian beam (i.e., one whose beam waist has the same width as that of the actual output beam) is calculated (ISO Std. 11146).

III. Results and Discussion

The purpose of the analysis is to investigate the nonlinear phenomena that influence the beam quality of tapered high-power laser diodes. This analysis will help to make design modifications in order to improve the brightness of these devices. The epitaxy for a typical 732-nm GaAs-based laser given in Table I was chosen for the purpose of this analysis. The cavity structures studied have a 4° gain-guided taper and a 3-μm-wide ridge waveguide. The lengths of the ridge waveguide and tapered gain sections are 0.75 and 1.25 mm, respectively. The rear facet reflectivity is 95%. The influences of the front facet reflectivity and the inclusion of a beam spoiler are studied.

As will be shown, the deterioration of the beam quality of the tapered laser results mainly from four phenomena, i.e., SHB, filamentation, optical pumping, and electrical overpumping.

TABLE I
EPITAXIAL STRUCTURE OF THE LASER CAVITY

Layer	Material	Thickness [nm]	Doping [cm^{-1}]	Refractive index
p-contact metal				
p-contact layer	GaAs		p+	3.741
p-cladding	$Al_{0.70}Ga_{0.30}As$		p	3.229
p-waveguide	$Al_{0.65}Ga_{0.35}As$	500	p	3.263
quantum well	$GaAs_{0.67}P_{0.33}$	9	n	3.585
n-waveguide	$Al_{0.65}Ga_{0.35}As$	500	n	3.263
n-cladding	$Al_{0.70}Ga_{0.30}As$		n	3.229
n-buffer+ substrate	GaAs		n	3.741
n-contact metal				

TABLE II
SIMULATION PARAMETERS

Material properites		
Band Offset $\Delta E_c/\Delta E_g$ (QW)	0.32	
Intraband relaxation time	0.1	ps
Electron capture time	3	ps
Hole capture time	1.2	ps
Auger coefficient	1.5E-30 (at RT)	cm^6s^{-1}
Band-gap renorm. coefficient	-0.00225e-05	eV
Free carrier absorption cross section	3E-18 (n); 7E-18 (p)	cm^2
BPM parameters		
Calculation area	2000 x 400	μm^2
Lateral step	0.1 – 0.4	μm
Longitudinal step	1 - 2	μm

The role of the first two effects on the deterioration of the beam quality at large output powers has been discussed extensively in the literature. However, the roles of optical pumping and electrical overpumping have not been properly explained in the context of tapered high-power laser cavities. Consequently, the SHB and filamentation effects will be discussed only briefly, before focusing on the optical pumping and electrical overpumping effects.

A. Comparison of the Experiment and Simulation

A number of experimental results have been gathered from 732-nm tapered laser diodes fabricated without beam spoilers, including light–current characteristics, near- and far-field patterns, and various beam quality parameters (i.e., M^2, beam divergence, astigmatism, and power content in the main lobe). As a result, it has been possible to carry out the extensive comparison between the numerical and the experimental results performed in this subsection.

The material parameters used in the simulations were taken from standard references [50], [51], when available. Typical parameters for GaAs also were used in the QW when GaAsP data were not found. Table II collects the most important parameters used as default in the simulations, which were kept unchanged throughout the simulations.

The comparison between experiments and simulations included a two-step fitting procedure. In the first step, the measured threshold currents and slope efficiencies of a set of broad-area lasers fabricated using the same epitaxial structure were compared with 1-D simulations performed with the laser simulator described in [24] and [26]. The fitting parameters were the trap density in the confinement region and the internal scattering losses. In the second step, the widths of the calculated and experimental far-field patterns for the tapered laser under study were compared. The proportionality constant relating the carrier induced index perturbation and the carrier density was used as a fit parameter, and a good matching was found using -2.7×10^{-11} $cm^{3/2}$ for the epitaxial structure analyzed in this paper. Simulations were also performed for different laser geometries (taper angle, cavity length) with the same epitaxial structure.

Fig. 3 shows a comparison between experimentally and numerically obtained light–current characteristics, M^2, power in the central lobe of the virtual source, astigmatism, and beam waist. The experimental beam parameters were obtained using the moving slit method. A good agreement is obtained between experiment and simulation for the light–current characteristics yielding both the same threshold current and slope efficiency. Similarly, a good agreement is observed between the measured and calculated values of power in the central lobe of the virtual source and the astigmatism. However, there is a discrepancy for the beam divergence and consequently for M^2, as discussed below.

Figs. 4–6 show the numerical and experimental near-field, and far-field patterns, and virtual source distribution at selected output powers. The near-field patterns agree quite well. The symmetry of the simulated patterns, as commented in Section II, is a result of the model assumptions. The experimental and numerical results both show the appearance of sidelobes and filamentation at larger output powers along with a gradual narrowing of the near-field pattern. The numerically and experimentally obtained far-field patterns also agree well. The appearance of sidelobes at larger output powers is seen in both the experimental and the numerical results and the widths of the measured and calculated far-field pattern agree well, particularly considering the experimental variation observed in the irregular peak behavior of these devices. The origins of the beam quality deterioration at high output power will be discussed in the following subsections. In the case of the virtual source, however, there are some discrepancies between experiment and modeling. Although both measurement and calculation show that the main lobe width does not depend on the output power, there is a difference in the actual value of the virtual source width. This discrepancy may be a combined effect of the 2-D effective index approximation, the limited numerical aperture of the imaging optics, and aberration of the optical wave front [52].

B. Filamentation and SHB

The phenomena of filamentation and hole burning are fairly well described in the literature, both in terms of theory and experiment for both broad-area lasers [27], [28], [31], [53] and tapered amplifiers [16]. The aim of this subsection is to identify and discuss the impact of these phenomena in the tapered laser diodes considered here.

Fig. 7 shows the photon and QW gain distributions for the laser diode described in Section III-A to illustrate the appearance of the SHB effect. The carrier density in the QW and the QW

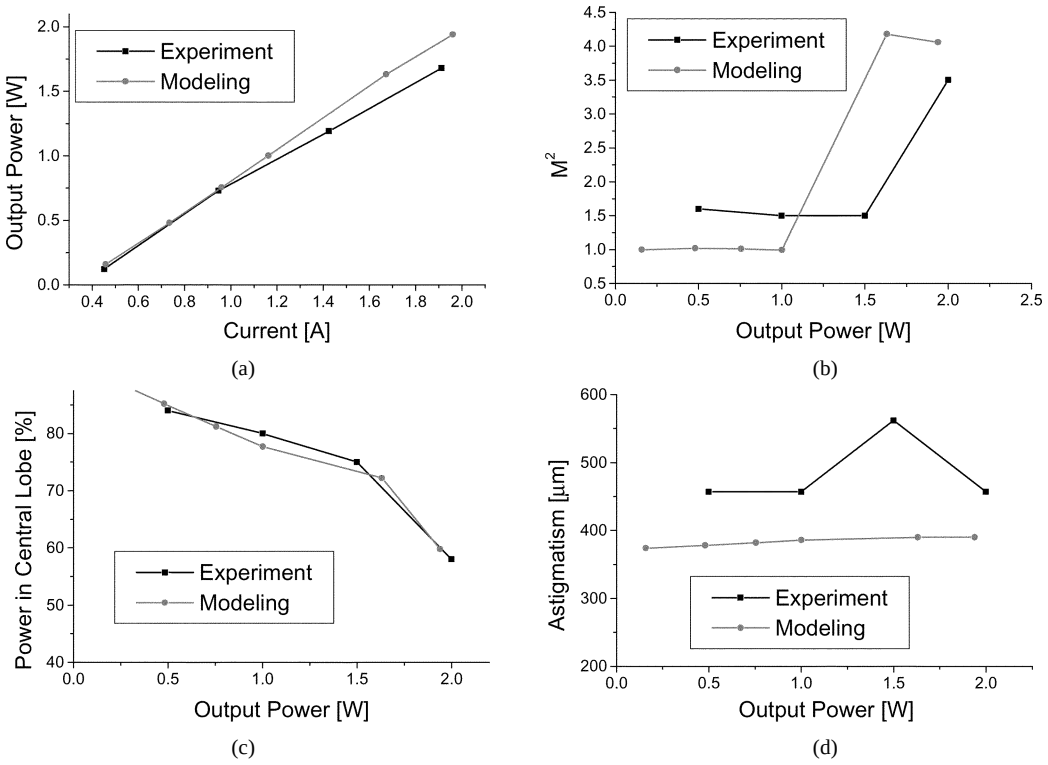

Fig. 3. Light–current characteristics and the dependence of beam divergence, M^2, power in central lobe of the virtual source, astigmatism, and beam waist on the output power. $L = 2$ mm, $L_{\mathrm{RW}} = 0.75$ mm, $W_{\mathrm{RW}} = 3\ \mu$m, $W_o = 90.3\ \mu$m, $R_{\mathrm{RW}} = 95\%$, $R_o = 1\%$, and $\Delta n_{\mathrm{eff}} = 0.008$.

gain are significantly reduced in the regions where photon density reaches local maximum, which is evidence of SHB. To visualize how the SHB effect influences filamentation, the carrier and photon densities, the refractive index perturbation, and the QW gain profile at the front facet of the device are all shown in Fig. 8. At low output powers, the carrier and photon densities are flat and no filamentation or SHB is observed. However, with increasing output power, a reduction in the carrier density appears in the regions where the photon density reaches a local maximum. This is accompanied by a reduction in the QW gain (SHB) and the formation of local waveguides, which coincide with the photon density pattern and are responsible for the filamentation effect [53]. The width of the central local waveguide decreases as the refractive index contrast increases with increasing output power. The narrowing of the central local waveguide is accompanied by sidelobe narrowing and a shift toward the center of the waveguide. In the next section, we will show that the SHB and filamentation effects are strongly enhanced by the optical pumping effect. The optical pumping degrades the filtering properties of the straight section and then triggers a positive feedback mechanism that gets an SHB effect, which results in filamentation.

C. Optical Pumping and Electrical Overpumping Effects

The optical pumping and electrical overpumping phenomena will be discussed in detail in this subsection, since they are important for proper understanding of the tapered laser diode behavior at large output powers.

The optical pumping phenomenon is found to cause a deterioration of the modal filtering efficiency of the ridge waveguide

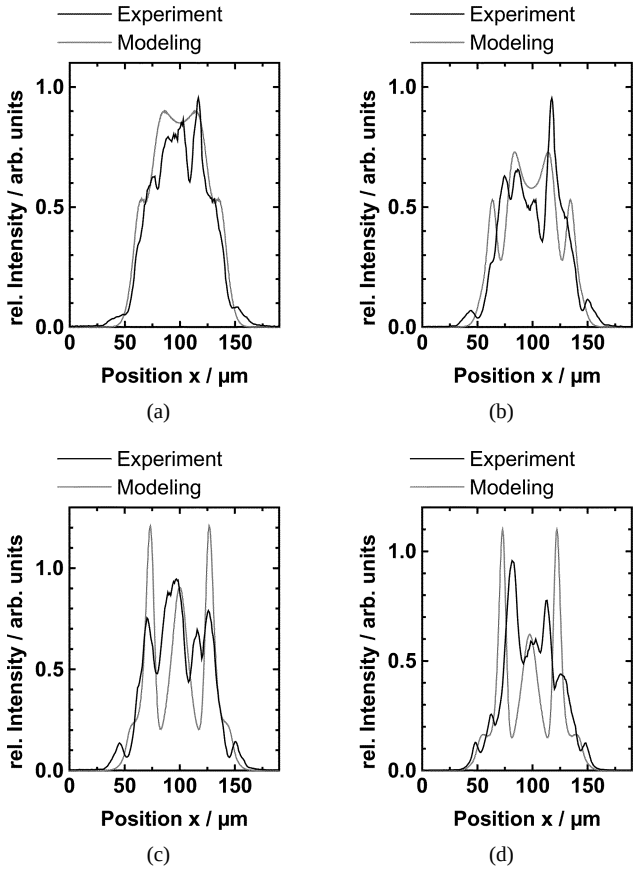

Fig. 4. Near-field power distributions (the same geometrical parameters as in Fig. 3). $R_{\mathrm{RW}} = 95\%$, $R_o = 1\%$. (a) $P = 0.5$ W, (b) $P = 1$ W, (c) $P = 1.5$ W, and (d) $P = 2$ W.

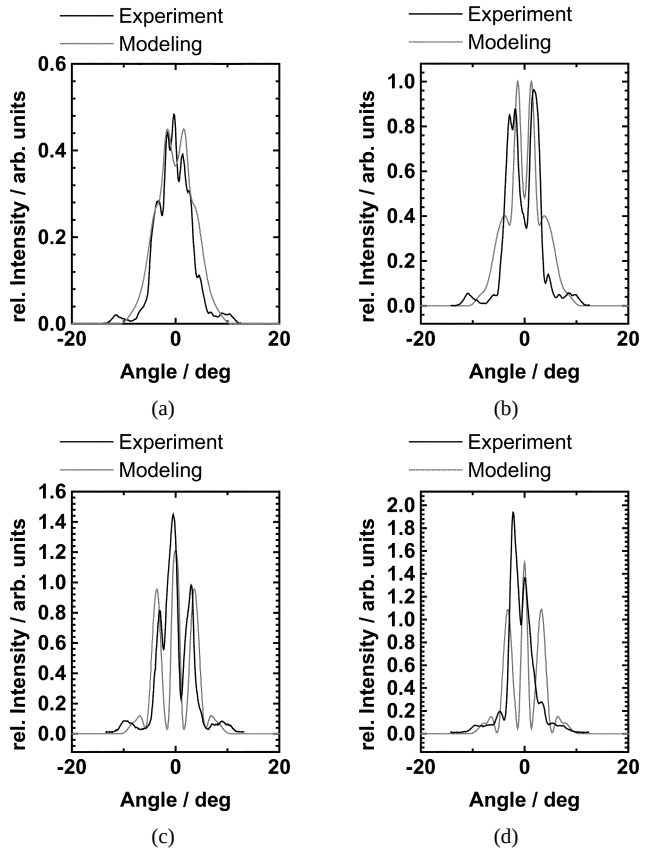

Fig. 5. Far-field power distributions (the same geometrical parameters as in Fig. 3). $R_{\mathrm{RW}} = 95\%$, $R_o = 1\%$. (a) $P = 0.5$ W, (b) $P = 1$ W, (c) $P = 1.5$ W, and (d) $P = 2$ W.

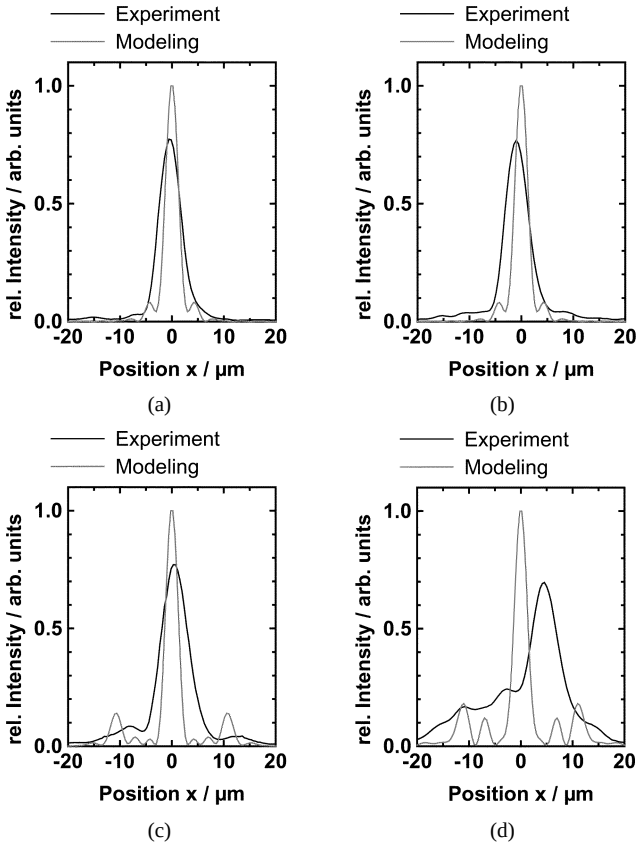

Fig. 6. Virtual source power distributions (the same geometrical parameters as in Fig. 3). $R_{\mathrm{RW}} = 95\%$, $R_o = 1\%$. (a) $P = 0.5$ W, (b) $P = 1$ W, (c) $P = 1.5$ W, and (d) $P = 2$ W.

section. As a result, the light scattered during back propagation can propagate to the rear facet, where it is reflected and can reach the tapered section. When this unfiltered light reaches the tapered amplifier, it can seed the formation of filaments. Fig. 9 shows the photon distribution of the backward wave in the cavity for the laser diode described in Section III-A at output powers of 0.2 and 1 W. The relative sizes of the sidelobes in the ridge waveguide section are much smaller at 0.2 W than at 1 W, showing that the filtering efficiency decreases with increasing output power. To investigate this phenomenon in more detail, the carrier and photon densities, refractive index perturbation, and QW gain at the rear facet of this device are shown in Fig. 10. The intensity of the scattered light in the regions adjacent to the ridge waveguide increases with increasing output power, providing optical pumping, which increases the local carrier density. When the region outside of the ridge waveguide approaches transparency, there is a strong decrease in the filtering efficiency of the straight section.

The role of the regions adjacent to the ridge waveguide can be understood in more detail as follows. The backward-propagating wave is strongly scattered by the tapered structure because of its curved phase front (which causes it to diverge). This scattering is particularly significant at the interface between the tapered and straight sections (Fig. 9). Consequently, a significant amount of the power in the backward-propagating wave is contained in higher order lateral modes, which pumps the electrically unpumped regions. After reflection at the rear facet, the amplified backward-propagating wave seeds the forward-propagating wave. The sidelobes propagate along the outside of the ridge waveguide and re-enter the electrically pumped region in the tapered section. Thus, if the angle of propagation of the sidelobes is smaller than the taper angle, they partly scatter from the taper, because the refractive index perturbation forms an antiguiding structure and form sidelobes in the near-field patterns (Fig. 4) that help seed the filamentation process. Hence, the optical pumping effect is identified as the source of the irregular beam pattern, which triggers SHB effects and, thus, filamentation.

The intensity of the optical pumping effect can be reduced by decreasing the front facet reflectivity, i.e., by decreasing the intensity of the backward wave. This idea is illustrated in Fig. 11, which compares the photon distribution in the same cavity for two values of front facet reflectivity: 1% (used in the previous calculations) and 0.1%. The lower front facet reflectivity clearly reduces the optical pumping effect, thereby delaying the degradation of the straight section filtering properties. The optical pumping effect can also be suppressed through the application of beam spoilers, as shown in Fig. 12. Fig. 13 shows the photon density distribution after the addition of a beam spoiler with a 6-μm aperture, positioned 100 μm from the rear facet. Again, the photon distribution and near-field profiles are strongly improved and the bleaching-induced effects have been reduced.

Beam spoilers are commonly used to improve the performance of tapered lasers with the explanation that they improve the spatial filtering [11], [15].

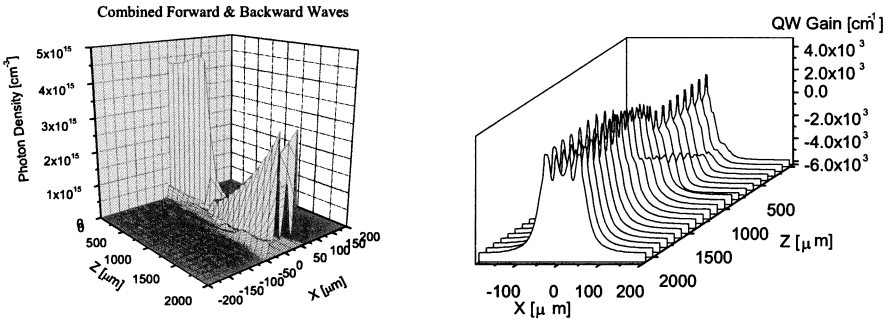

Fig. 7. Simulated photon and carrier density distributions at $P = 1$ W (the same geometrical parameters as in Fig. 3). $R_{\rm RW} = 95\%$, $R_o = 1\%$.

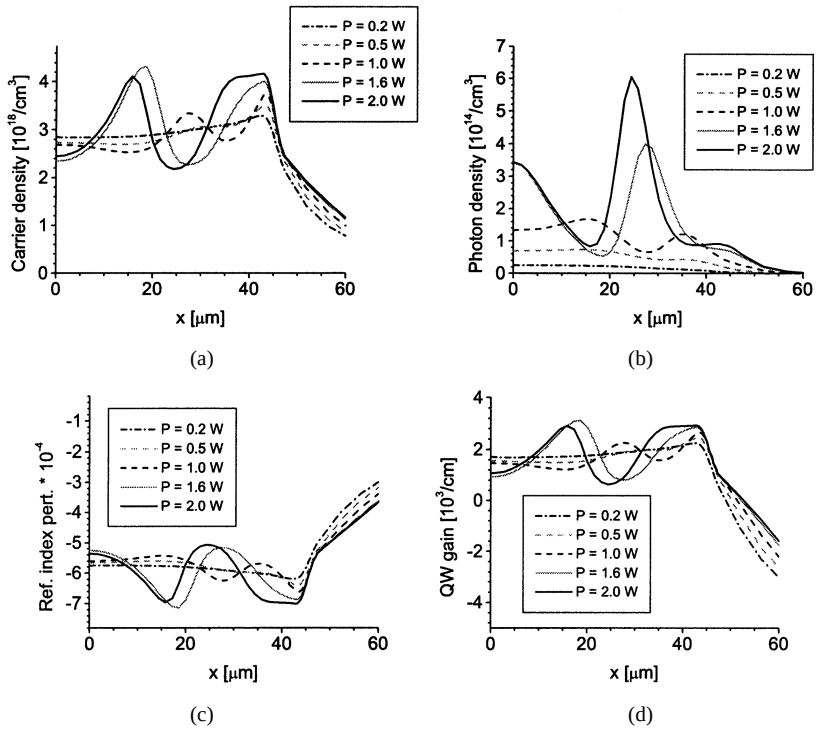

Fig. 8. Simulated photon density, carrier density, refractive index perturbation, and gain distributions at the front facet (the same geometrical parameters as in Fig. 3). $R_{\rm RW} = 95\%$, $R_o = 1\%$. Note that due to symmetry, only one half of the structure is included.

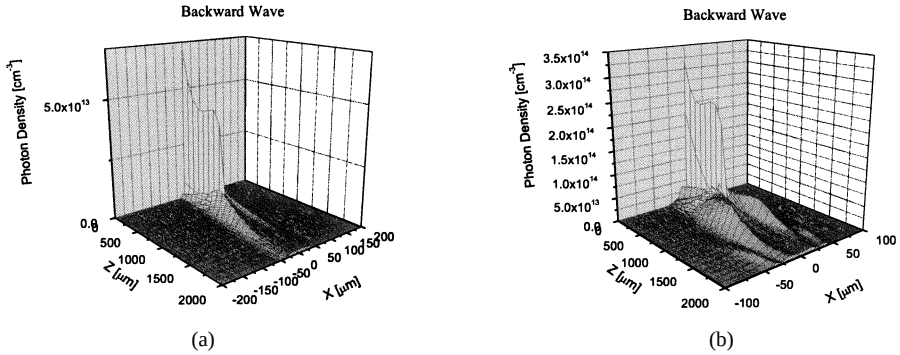

Fig. 9. Simulated photon distributions at (a) $P = 0.2$ W and (b) $P = 1$ W (the same geometrical parameters as in Fig. 3). $R_{\rm RW} = 95\%$, $R_o = 1\%$.

Similarly, lower front facet reflectivities have been observed to improve the output beam quality [26], [54], but again, no connection was made to the role of optical pumping in the straight section.

Finally, we mention the last effect—electrical overpumping. Electrical overpumping becomes most apparent when the optical pumping effect is suppressed by one of the methods described above. In Fig. 14, we compare the carrier and photon densities, the refractive index perturbation, and the QW gain at the front facet of the same device. The optical pumping is suppressed by a beam spoiler with a 6-μm aperture, positioned 100 μm from the rear facet. The carrier density increases rapidly with output

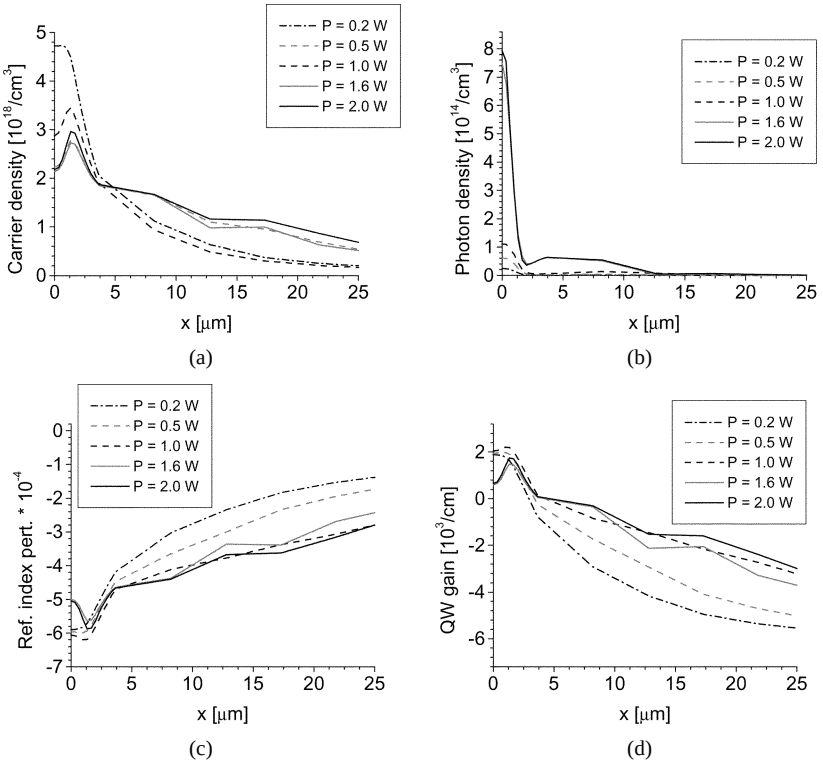

Fig. 10. Simulated photon density, carrier density, refractive index perturbation, and gain distributions at the rear facet (the same geometrical parameters as in Fig. 3). $R_{\mathrm{RW}} = 95\%$, $R_o = 1\%$. Note that due to symmetry, only one half of the structure is included.

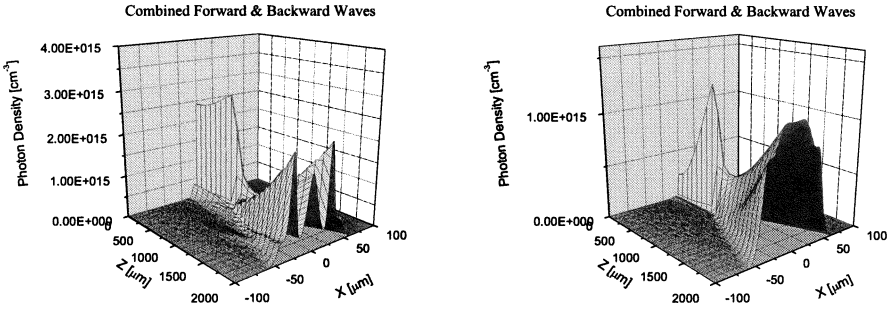

Fig. 11. Simulated photon density distributions at $P = 1$ W (the same geometrical parameters as in Fig. 3). $R_{\mathrm{RW}} = 95\%$. (a) $R_o = 1\%$ and (b) $R_o = 0.1\%$.

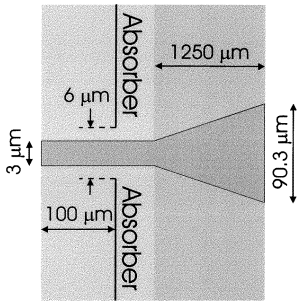

Fig. 12. Laser cavity geometry with a beam spoiler.

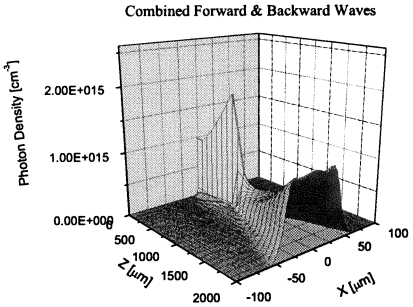

Fig. 13. Simulated photon density distribution for a cavity with a beam spoiler at $P = 1$ W (the same geometrical parameters as in Fig. 3). $R_{\mathrm{RW}} = 95\%$, $R_o = 1\%$.

power in the regions of low photon density (i.e., at the edges of the taper), resulting in a large increase of the local gain and a decrease in the local refractive index. As a result, a shoulder builds up in the photon distribution, which ultimately takes the shape of small local peaks at the outer edges of the photon distribution. Electrical overpumping has been recognized in the literature [29], [30], [32], and the use of patterned contacts has been proposed to tailor the current injection appropriately [33]. However, as shown here, the true impact of electrical

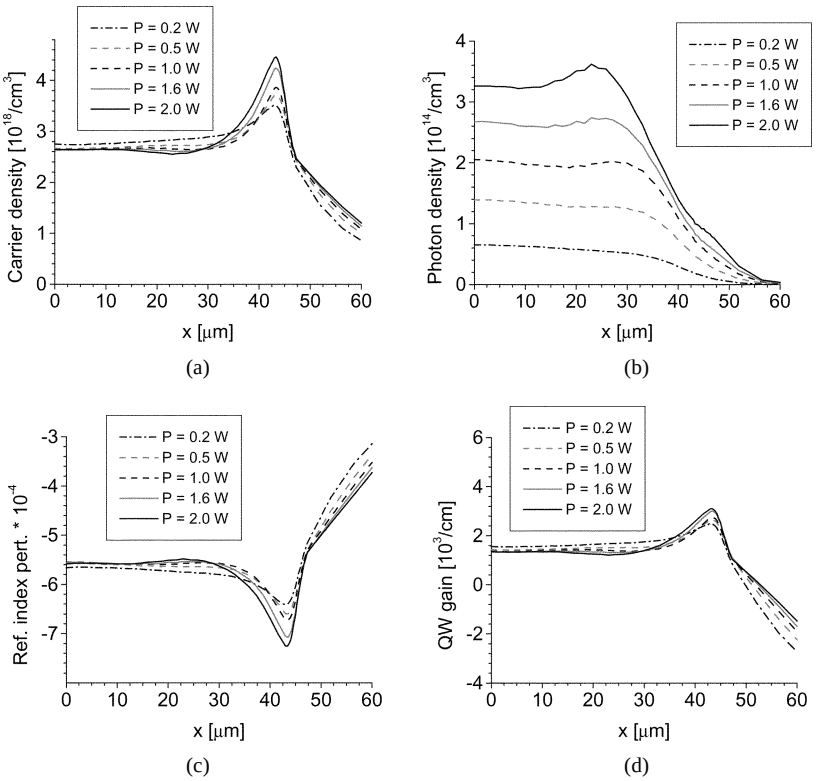

Fig. 14. Simulated photon and carrier densities, refractive index perturbation, and gain distributions at the front facet for the laser cavity with a beam spoiler (the same geometrical parameters as in Fig. 3). $R_{\mathrm{RW}} = 95\%$, $R_o = 1\%$. Note that due to symmetry, only one half of the structure is included.

overpumping has generally been overestimated because of the presence of the optical pumping.

IV. Conclusion

An efficient and predictive design tool for high-power tapered lasers has been developed, which only relies on a simple independent adjustable parameter: the constant relating of the refractive index perturbation to changes in the carrier density in the QW. All other materials parameters are either taken from standard references or from measurements on broad-area lasers with the same epitaxial material.

The model has been applied to 732-nm high-power tapered lasers designed for fiber-coupled photodynamic therapy applications. The numerical results agree well with the experiment over a wide range of operating conditions. Although this model cannot be used to investigate complex dynamic processes in semiconductor lasers, it is computationally efficient and is capable of predictive modeling those physical effects and properties which are most important for applications of high-power laser diodes. In particular, the near- and far-field patterns and their evolution with power are predicted correctly. The model has permitted the identification of four key phenomena influencing the quality of the output beam: SHB, filamentation, optical pumping, and electrical overpumping.

The SHB and filamentation effects behave similarly to the results reported in the literature. The suppression of the optical pumping effect is crucial for the improvement of the beam quality of tapered lasers at high output powers. The electrical overpumping effect, however, only becomes apparent once the optical pumping effect has been suppressed through the use of a beam spoiler.

References

[1] G. P. Agrawal, *Fiber-Optic Communication Systems*. New York: Wiley, 1997.

[2] *IEEE J. Select. Topics Quantum Electron. (Special Issue on Lasers in Medicine and Biology)*, vol. 2, Dec. 1996.

[3] W. Schulz and R. Poprawe, "Manufacturing with novel high-power diode lasers," *IEEE J. Select. Topics Quantum Electron.*, vol. 6, pp. 696–705, July-Aug. 2000.

[4] D. Stryckman, G. Rousseau, M. D'Auteuil, and N. McCarthy, "Improvement of lateral-mode discrimination of broad-area diode lasers with profiled reflectivity output facet," *Appl. Opt.*, vol. 35, pp. 5955–5959, 1996.

[5] F. Camacho, C. J. Hamilton, K. McIlvaney, A. C. Bryce, and J. H. Marsh, "Laser structure for generating high optical power in a singlemode waveguide," *Electron. Lett.*, vol. 34, pp. 460–461, Mar. 1998.

[6] C. Zmudzinski, D. Botez, L. J. Mawst, A. Bhattacharya, M. Nesnidal, and R. F. Nabiev, "Three-core ARROW-type diode laser: Novel high-power, single-mode device, and effective master oscillator for flared antiguided MOPA's," *IEEE J. Select. Topics Quantum Electron.*, vol. 2, pp. 129–137, June 1995.

[7] R. J. Lang, K. M. Dzurko, A. Hardy, S. Demars, A. Schoenfelder, and D. F. Welch, "Theory of grating-confined broad-area lasers," *IEEE J. Quantum Electron.*, vol. 34, pp. 2197–2210, Nov. 1998.

[8] S. O'Brien, D. F. Welch, R. A. Parke, D. Mehuys, K. Dzurko, R. J. Lang, R. Waarts, and D. Scifres, "Operating characteristics of high-power monolithically integrated flared amplifier master oscillator power amplifier," *IEEE J. Quantum Electron.*, vol. 29, pp. 2052–2057, June 1993.

[9] L. M. Tilton, G. C. Dente, A. H. Paxton, J. Cser, R. K. DeFreez, C. E. Moeller, and D. Depatie, "High power, nearly diffraction-limited output from a semiconductor laser with an unstable resonator," *IEEE J. Quantum Electron.*, vol. 27, pp. 2098–2108, Sept. 1991.

[10] D. Mehuys, D. F. Welch, and D. Scifres, "1 W CW, diffraction-limited, tunable external-cavity semiconductor laser," *Electron. Lett.*, vol. 29, pp. 1254–1255, July 1993.

[11] J. P. Donnelly, J. N. Walpole, S. H. Groves, R. J. Bailey, L. J. Missaggia, A. Napoleone, R. E. Reeder, and C. C. Cook, "1.5 μm tapered-gain-region lasers with high-CW output powers," *IEEE Photon. Technol. Lett.*, vol. 10, pp. 1377–1379, Oct. 1998.

[12] F. J. Wilson, J. J. Lewandowski, B. K. Nayar, D. J. Robbins, P. J. Williams, N. Carr, and F. O. Robson, "9.5 W CW output power from high brightness 980 nm InGaAs/AlGaAs tapered laser arrays," *Electron. Lett.*, vol. 35, pp. 434–435, 1999.

[13] S. Sujecki, J. Wykes, P. Sewell, A. Vukovic, T. M. Benson, E. C. Larkins, L. Borruel, and I. Esquivias, "Optical properties of tapered laser cavities," *Proc. Inst. Elect. Eng.–Optoelectron.*, to be published.

[14] K. A. Williams, R. W. Penty, I. H. White, D. J. Robbins, F. J. Wilson, J. J. Lewandowski, and B. K. Nayar, "Design of high-brightness tapered laser arrays," *IEEE J. Select. Topics Quantum Electron.*, vol. 5, pp. 822–831, May-June 1999.

[15] S. Mariojouls, S. Margott, A. Schmitt, M. Mikulla, J. Braunstein, G. Weimann, F. Lozes, and S. Bonnefont, "Modeling of the performance of high-brightness tapered lasers," *Proc. SPIE*, vol. 3944, pp. 395–406, 2000.

[16] S. Ramanujan and H. G. Winful, "Spontaneous emission induced filamentation in flared amplifiers," *IEEE J. Quantum Electron.*, vol. 32, pp. 784–789, May 1996.

[17] E. Gering, O. Hess, and R. Wallenstein, "Modeling of the performance of high-power diode amplifier systems with on opto-thermal microscopic spatio-temporal theory," *IEEE J. Quantum Electron.*, vol. 35, pp. 320–331, Mar. 1999.

[18] J. Piprek and S. Nakamura, "Physics of high-power InGaN/GaN lasers," *Proc. Inst. Elect. Eng., Optoelectron.*, vol. 149, pp. 145–151, 2002.

[19] B. Sumpf, R. Hülsewede, G. Erbert, C. Dzionk, J. Fricke, A. Knauer, W. Pittroff, P. Ressel, J. Sebastian, H. Wenzel, and G. Tränkle, "High-brightness 735 nm tapered diode lasers," *Electron. Lett.*, vol. 38, pp. 183–184, Feb. 2002.

[20] L. Borruel, S. Sujecki, M. Krakowski, B. Sumpf, P. Moreno, J. Wykes, S. C. Auzanneau, G. Erbert, D. Rodríguez, P. Sewell, M. Calligaro, H. Wenzel, T. M. Benson, E. C. Larkins, and I. Esquivias, "High brightness tapered lasers at 732 nm and 975 nm: Experiments and numerical analysis," in *Proc. IEEE Int. Semiconductor Laser Conf.*, Germany, Sept. 2002.

[21] R. F. Kazarinov, C. H. Henry, and R. A. Logan, "Longitudinal mode self-stabilization in semiconductor lasers," *J. Appl. Phys.*, vol. 53, pp. 4631–4643, 1982.

[22] C. Z. Ning, J. V. Moloney, A. Egan, and R. A. Indik, "A first-principles fully space-time resolved model of a semiconductor laser model," *J. Opt. B, Quantum Semiclassical Optics*, vol. 9, p. 681, 1997.

[23] G. R. Hadley, "Numerical simulation of microcavity diode lasers using FDTD methods on a triangular grid," in *Proc. Int. Workshop Numerical Modeling*, Hagen, Germany, 2001.

[24] H. Wenzel, B. Sumpf, and G. Erbert, "High-brightness diode lasers," *Comptes Rendue Physique*, submitted for publication.

[25] M. Gruppen and K. Hess, "Simulation of carrier transport and nonlinearities in quantum well laser diodes," *IEEE J. Quantum Electron.*, vol. 34, pp. 120–139, Jan. 1998.

[26] J. V. Moloney, R. A. Indik, and C. Z. Nong, "Full space time simulation for high brightness semiconductor lasers," *IEEE Photon. Technol. Lett.*, vol. 9, pp. 731–733, June 1997.

[27] G. H. B. Thompson, *Physics of Semiconductor Laser Devices*. New York: Wiley, 1990.

[28] A. H. Paxton and G. C. Dente, "Filament formation in semiconductor laser gain regions," *J. Appl. Phys.*, vol. 70, pp. 2921–2925, 1991.

[29] L. Goldberg, M. R. Surette, and D. Mehuys, "Filament formation in a tapered GaAlAs optical ampiflier," *Appl. Phys. Lett.*, vol. 62, no. 19, pp. 2304–2306, 1993.

[30] A. Egan, C. Z. Ning, J. V. Moloney, R. A. Indik, M. W. Wright, D. J. Bossert, and J. G. McInerney, "Dynamic instabilities in master oscillator power amplifier semiconductor lasers," *IEEE J. Quantum Electron.*, vol. 34, pp. 166–170, Jan. 1998.

[31] Z. Dai, R. Michalzik, P. Unger, and K. J. Ebeling, "Numerical simulation of broad-area high-power semiconductor laser amplifiers," *IEEE J. Quantum Electron.*, vol. 33, pp. 2240–2254, Dec. 1997.

[32] P. M. Smowton and P. Blood, "The differential efficiency of quantum well lasers," *IEEE J. Select. Topics Quantum Electron.*, vol. 3, pp. 491–498, Apr. 1997.

[33] P. Salet, F. Gerard, T. Fillion, A. Pinquier, J. L. Gentner, S. Delpine, and P. Doussiere, "1.1 W continuous wave 1480 nm semiconductor lasers with distributed electrodes for mode shaping," *IEEE Photon. Technol. Lett.*, vol. 10, pp. 1706–1708, Dec. 1998.

[34] B. E. A. Saleh and M. C. Teich, *Fundamentals of Photonics*. New York: Wiley, 1991.

[35] J. Arias, L. Borruel, B. Romero, I. Esquivias, J. P. Hirtz, J. Nagle, and P. Collot, "One-dimensional simulation of high power laser diode structures," in *NUSOD'02*, Zurich, Switzerland.

[36] L. Borruel, S. Sujecki, I. Esquivias, J. Wykes, P. Sewell, T. M. Benson, E. C. Larkins, J. Arias, and B. Romero, "A self consistent electrical, thermal and optical model of high brightness tapered lasers," in *Proc. SPIE Photonics West*, San Jose, CA, 2002.

[37] HAROLD, Photon Design Ltd., U.K..

[38] J. Arias, L. Borruel, B. Romero, G. Batko, I. Esquivias, R. G.R. Gómez Alcalá, J. P. Hirtz, J. Nagle, and P. Collot, "One-dimensional simulation of high power laser diode structures," *IEEE J. Select. Topics Quantum Electron.*, submitted for publication.

[39] B. Romero, I. Esquivias, S. Weisser, E. C. Larkins, and J. Rosenzweig, "Carrier capture and escape processes in $In_{0.25}Ga_{0.75}As$–GaAs quantum-well lasers," *IEEE Photon. Technol. Lett.*, vol. 7, pp. 779–801, July 1999.

[40] B. Romero, J. Arias, I. Esquivias, and M. Cada, "Simple model for calculating the ratio of the carrier capture and escape times in quantum-well lasers," *Appl. Phys. Lett.*, vol. 76, no. 12, pp. 1504–1506, 2000.

[41] L. Borruel, J. Arias, B. Romero, and I. Esquivias, "Incorporation of carrier capture and escape processes into a self-consistent cw model for quantum well lasers," *Microelectron. J.*, vol. 34, no. 5–8, pp. 675–677, 2003.

[42] L. A. Coldren and S. W. Corzine, *Diode Lasers and Photonic Integrated Circuits*. New York: Wiley, 1995.

[43] H. Wenzel, G. Erbert, and P. M. Enders, "Improved theory of the refractive-index change in quantum-well lasers," *IEEE J. Select. Topics Quantum Electron.*, vol. 5, pp. 637–642, May-June 1999.

[44] M. S. Stern, "Semi-vectorial polarized finite difference method for optical waveguides with arbitrary index profiles," *Proc. Inst. Elect. Eng.*, vol. 135, pp. 56–63, 1988.

[45] J. G. Wykes, S. Sujecki, P. Sewell, T. M. Benson, E. C. Larkins, I. Esquivias, and L. Borruel, "Convergence behavior of coupled electromagnetic/thermal/electronic high power laser models," in *Proc. IEE Computation in Electromagnetics Conf.*, Bournemouth, U.K., Apr. 8–11, 2002.

[46] G. P. Agrawal, "Fast-Fourier-Transform based beam-propagation model for stripe-geometry semiconductor laser: Inclusion of axial effects," *J. Appl. Phys.*, vol. 56, no. 11, pp. 3100–3109, 1984.

[47] T. Anada, T. Hokazono, T. Hiraoka, H. Jui-Pang, T. M. Benson, and P. Sewell, "Very-wide-angle beam propagation methods for integrated optical circuits," *IEICE Trans. Electron.*, vol. E82-C, pp. 1154–1158, 1999.

[48] T. M. Benson, P. Sewell, and A. Vukovic, "Interfacing the finite difference beam propagation method with fast semi-analytic techniques," in *Proc. OSA Integrated Photonics Research Symp.*, Quebec, QC, Canada, 2000, pp. 48–50.

[49] L. B. Felsen and N. Marcuvitz, *Radiation and Scattering of Waves*. Oxford, U.K.: Oxford Univ. Press, 1994.

[50] S. Adachi, Ed., *Properties of Aluminum Gallium Arsenide*. London, U.K.: Inspec, 1993.

[51] S. Vurgaftman, J. R. Meyer, and L. R. Ram-Mohan, "Band parameters for III-V compound semiconductors and their alloys," *J. Appl. Phys.*, vol. 89, pp. 5815–5875, 2000.

[52] S. P. Morgan, private communication.

[53] J. R. Marciante and G. P. Agrawal, "Nonlinear mechanisms of filamentation in broad-area semiconductor lasers," *IEEE J. Quantum Electron.*, vol. 32, pp. 590–597, Apr. 1996.

[54] G. Levy and A. Hardy, "Chaotic effects in flared lasers: A numerical analysis," *IEEE J. Quantum Electron.*, vol. 33, pp. 26–32, Jan. 1997.

Slawomir Sujecki received the M.Sc. and Ph.D. degrees in electronic engineering from the Warsaw University of Technology, Warsaw, Poland, in 1993 and 1997, respectively.

He spent one academic year (1994–1995) at the Technische Universität Berlin, Berlin, Germany, as a DAAD Fellow and two years (1996–1998) at the University of Nottingham, Nottingham, U.K., as a British Council and then Royal Society/Wolfson Foundation Fellow. In 1998, he was with Kielce University of Technology, Kielce, Poland, and in 1999 he joined the National Institute of Telecommunications, Warsaw, Poland. Since April 200l, he has been with the School of Electrical and Electronic Engineering, University of Nottingham.

Luis Borruel was born in Madrid, Spain, in 1972. He received the B.Eng. degree in telecommunications from Universidad Politécnica de Madrid, Madrid, Spain, in 1994 and the M.Sc. degree in physics from the Universidad Nacional de Educatión a Distancia (UNED), Spain, in 2000. He is currently working toward the Ph.D. degree at the Universidad Politécnica de Madrid.

In 1998, he joined the Laser Diode group in the Photonics Technology Department at the Universidad Politécnica de Madrid. After working on piezoelectric effects in InGaAs QW lasers, his current research interests are in high-brightness laser simulation, optimization, and characterization.

James Wykes received the M.Eng. degree in electronic engineering with first class honors from the University of Nottingham, Nottingham, U.K., in 2000, where he is currently pursuing the Ph.D. degree in the School of Electrical and Electronic Engineering.

His work is based on the development of advanced numerical modeling tools for the design and optimization of high-brightness tapered lasers.

Pablo Moreno was born in Spain in 1978. He received the degree in physics from the University Complutense of Madrid, Madrid, Spain, in 2002.

From July 2001 to October 2002, he was a Research Assistant in the Photonic Technology Department, Universidad Politécnica de Madrid. Besides high-power semiconductor lasers, he is presently engaged in research on monolithic mode-locked lasers at high repetition rates.

Bernd Sumpf was born in Berlin, Germany, in 1958. He received the Dipl. degree in physics in 1981 and the Ph.D. degree in 1987 from the Humboldt-Universität, Berlin, for his work on lead salt diode lasers for spectroscopic applications.

From 1993 to 1997, he worked at the Technische Universität Berlin on high-resolution spectroscopy and difference-frequency generation. In 1997, he received the postdoctoral lecture qualification. Since 2000, he has been working at the Ferdinand-Braun-Institut for Höchstfrequenztechnik, Berlin, on high-brightness diode lasers.

Phillip Sewell was born in London, U.K., in 1965. He received the B.Sc. degree in electrical and electronic engineering with first class honors and the Ph.D. degree from the University of Bath, Bath, U.K., in 1988 and 1991, respectively.

From 1991 to 1993, he was an S.E.R.C. Postdoctoral Fellow at the University of Ancona, Ancona, Italy. Since 1993, he has been a Lecturer, and from 2001 a Reader, in the School of Electrical and Electronic Engineering, University of Nottingham, Nottingham, U.K. His research interests involve analytical and numerical modeling of electromagnetic problems, with application to optoelectronics, microwaves, and electrical machines.

Hans Wenzel received the Dipl. and Ph.D. degrees in physics from Humboldt University, Berlin, Germany, in 1986 and 1991, respectively. His thesis dealt with the electrooptical modeling of semiconductor lasers.

From 1991 to 1994, he was involved in a research project on the three-dimensional simulation of DFB lasers. In 1994, he joined the Ferdinand-Braun-Institut für Höchstfrequenztechnik, Berlin, Germany, where he is engaged in the development of high-power semiconductor lasers including DFB lasers.

Trevor M. Benson was born in Sheffield, U.K., in 1958. He received the first class honors degree in physics and the Ph.D. degree in electronic and electrical engineering from The University of Sheffield, Sheffield, U.K., in 1979 and 1982, respectively.

After spending more than six years as a Lecturer at University College Cardiff, Wales, U.K., he joined the University of Nottingham, Nottingham, U.K., as a Senior Lecturer in Electrical and Electronic Engineering in 1989. He was promoted to the posts of Reader in Photonics in 1994 and Professor of Optoelectronics in 1996. His present research interests include experimental and numerical studies of electromagnetic fields and waves, with particular emphasis on propagation in optical waveguides and lasers, silicon based photonic circuits, and electromagnetic compatibility.

Goetz Erbert received the Dipl. degree in physics from Humboldt University, Berlin, Germany, in 1973 and the Ph.D. degree in physics from the Academy of Sciences of the German Democratic Republic, Berlin, in 1990.

From 1973 to 1991, he worked at the Academy of Sciences on integrated optics, dynamic holographic gratings in semiconductors, and semiconductor lasers. In 1992, he joined the Ferdinand-Braun-Institut, Berlin. Since 1996, he has been responsible for the optoelectronic activities at the institute. He is working on high-power, high-brightness semiconductor lasers based on GaAs.

Ignacio Esquivias was born in Madrid, Spain, in 1955. He received the M.Sc. and Ph.D. degrees in electronic engineering from the Polytechnical University of Madrid, Madrid, Spain, in 1977 and 1983, respectively.

In 1984, he became an Associate Professor with the Department of Electronic Technology at the Polytechnical University of Madrid. From 1990 to 1992, he was a Visiting Scientist at the Fraunhofer Institute for Applied Solid State Physics, Freiburg, Germany. In 1992, he returned to his position at the Polytechnical University of Madrid, becoming Full Professor in 2001 in the Department of Photonic Technology. His research activity has been always related with optoelectronic materials and devices (polycrystalline silicon solar cells, HgCdTe and HgZnTe for infrared detectors). Since 1991, he has been working in characterization and modeling of laser diodes for high-speed and high-power applications.

Eric C. Larkins received the B.S.E.E. degree from Cornell University, Ithaca, NY, in 1980 and the M.S.E.E. and Ph.D. E.E degrees from Stanford University, Stanford, CA, in 1985 and 1991, respectively. He pursued his Ph.D. research on light-emitting heterostructure thyristors and molecular beam epitaxy, receiving full support from 1985 as a Kodak Fellow.

From 1991 to 1994, he was a visiting scientist at the Fraunhofer Institute for Applied Solid State Physics, Freiburg, Germany, where he worked on high-speed laser diodes, optical modulators, and MSM and intersubband photodetectors. He joined the School of Electrical and Electronic Engineering at the University of Nottingham, Nottingham, U.K., as Lecturer in 1994 and was appointed Professor of Optoelectronics in 2002. His current research interests include high-power laser diodes, functional photonics, and new optical materials.